university of groningen / faculty of science and engineering

Automating the Analysis of Transition Edge Sensors in FDM Systems

Bachelor Thesis Physics

Author:
Tom van Rees

SRON Researcher:
dr. Damian Audley

Supervisor:
dr. Myroslav Kavatsyuk

Abstract

The existing software available to automatically analyze current-voltage curves from a single transition edge sensors (TES) was extended to include new methods to analyze data from the frequency domain multiplexing setup. This new software version is able to plot a grid image containing the absorbed power for multiple pixels and the Joule power for different black body temperatures for a specific pixel.

Furthermore, it utilizes a different fitting function which leads to more accurate parameter values, like the normal resistance, and is less prone to small errors. The software meets the demands specified and is fitted with debug options to observe the intermediary results for trouble shooting.

November 26, 2021

Contents

1 Introduction

Transition edge sensors (TES) are state of the art cryogenic calorimeters in the infrared and x-ray regime. SRON uses multiple TES sensors together to reach high-resolution spectroscopy, useful for particle detection in space telescopes. They are planned to be used in the Athena telescope, which will study the growing process of black holes and the clustering of galaxies [1]. On board of the ATHENA telescope is the X-ray Integral Field Unit (X-IFU), which will consist of thousands of TES sensors with higher energy resolutions than previous space telescopes [2].

The analysis of the data provided by a single TES detector has been automatized by Callum Blair [3]. However, it only works on data sets from a single TES device. Single TES detector setups generate double sided IV curves, more information can be found in Callum's Thesis. I will work on the automation of the analysis for single sided IV curves, which allows systems with multiple connected TES devices to be analyzed.

The software will be build upon the previous version, and the additional features will follow the following guidelines:

- The software should perform similarly as before when analyzing double sided IV curves.
- The software should not take up large amounts of computing power, to remain its ability to analyse large amounts of data sets.
- The software should be able to analyze single sided IV curves coming from the FDM setup.

Together with these guidelines, I will take a look if the current phase data affects the system.

Extending the software is necessary as manual analysis can take multiple minutes for each individual dataset, leading up to hours of work for a few measurements. Automating this process frees up time to work on the setup itself and look more in-depth at the final results.

2 Theory

A transition edge sensor (TES) is a state of the art cryogenic particle detector. The setup is complicated and built upon the knowledge of multiple domains of physics. TES are mostly used for detection in the x-ray and IR domains because of its unparalleled accuracy [4]. Superconductivity is mainly responsible for the high energy resolution of this device.

Superconductors are materials that have zero resistance below a critical temperature T_c. This phenomenon arises due to cooper pairs, which are described in the BCS theory. The movement of one electron attracts the other, and hence they travel as a pair throughout the superconductor with less scattering [5]. This leads to a resistance of 0 Ω. Cooper pairs have weak bonds, which can easily be broken at room temperature. These weak bonds also lead to a sharp increase in resistance when transitioning from below T_c to above.

2.1 Mechanisms of a TES

By keeping the TES near superconducting temperatures, it becomes highly sensitive to changes in temperature, caused by incoming photons. After a photon has hit the surface, the temperature rises above its critical temperature and the additional resistance changes

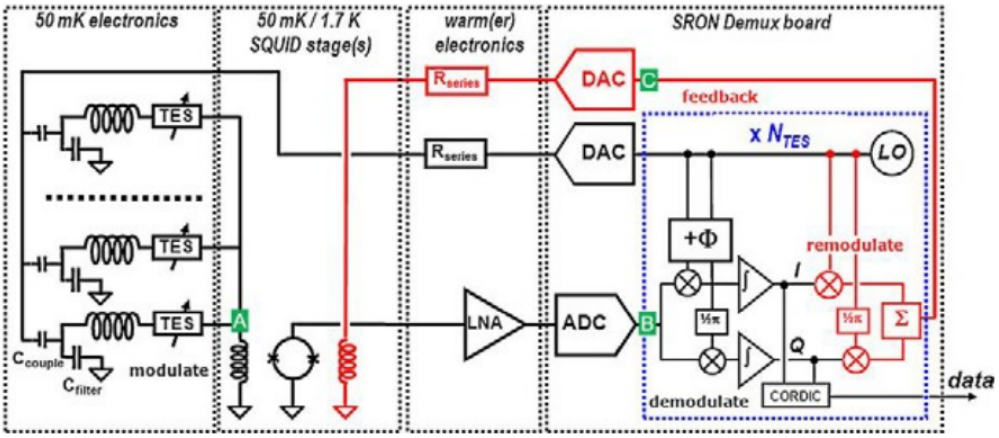

Figure 1: Electrical Setup of the Frequency Domain Multiplexing system [8].

the current and voltage. This is called a phase transition and the output of this transition is measured. All read out is done with a Superconducting QuantUm Interference Device (SQUID) ammeter, which measures extremely small magnetic fields in superconducting loops. These devices also allow for negative electrothermal feedback, returning the system back to its previous thermal state [6], instead of increasingly heating up due to Joule heating via the higher currents.

Previously Field Effect Transistors (FET) were used to measure the subtle magnetic fields, but they suffer from positive thermal feedback and hence are not feasible for continuous measurements.

2.2 Frequency Domain Multiplexing

SQUIDs also allow for creating large arrays of TES sensors working together, which is called multiplexing [7]. Large arrays of TES sensors are useful for detecting photons rays and creating more informative images of black body sources in space.

Multiple TES devices are connected to a single SQUID. This can be done in multiple ways, one of which utilizes the frequency of the signal sent out by an AC-biased voltage source. Such systems are called Frequency Domain Multiplexed (FDM) systems. Each TES is connected to an LC-circuit, sensitive to a specific frequency [8]. Figure 1 below shows the setup used by SRON and how the components are connected.

The signals are put together and the SQUID can read out the data for each individual TES detector utilizing the difference in frequency. Each TES detector is called a pixel, as they later will be used to display images where each detector provides the data for a single pixel of an image.

3 Experimental Setup

The setup of the whole apparatus can be seen in figure 2.

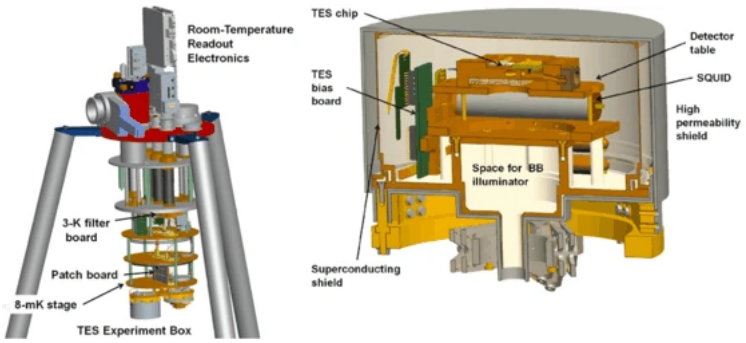

Figure 2: *(Left)* Display of the total setup without the shields that protect against the heat and magnetic fields. The stages show the differences in temperature during measurements. *(Right)* Cross section of the TES experiment box, found on the lower side on the left picture [9].

The setup within the borders of the tripod is housed within a heat shield, to keep the equipment inside at temperatures below 3 K to 8 mK, dependent upon the stage, and protect the electronics from interfering magnetic fields. Cryogenic generators are located outside the apparatus and cool a mixture of Helium-4 and Helium-3 gas, which is inserted into the machine via cables. All readout to a computer is performed at room temperature at the top of the setup. Going down from there, the temperature between boards gradually decreases down to 8 mK. The TES experiment box contains the TES chips, placed on the detector table. The TES bias board provides the AC signal for all TES chips, while the readout is done by the SQUID ammeter on the other side, to prevent interference from the bias board. Below the detector table any black body illuminator can be placed for calibration and testing of the system.

3.1 Electronics and Formulas

All TES sensors are connected to a controlled AC voltage bias source and to an LC-filter. The bias voltage V_{bias} is read out by the SQUID, together with the current phase angle. The feedback voltage V_{fb} is generated by a feedback loop and also read out by the SQUID. The shunt resistor R_{shunt} is a relatively large resistance ($\sim$MΩ) to stabilize the current going through the system. Leftover resistance is called R_{stray} or R_{par}, which is unknown beforehand but can be calculated. Another important parameter is the feedback correction factor F_{corr}, which is different for each TES.

The first calculated metric of the system is the *gain* of the system, calculated as $gain = \frac{1}{R_{fb} \cdot M_{ratio}}$. M_{ratio} is defined as the ratio of numbers of coils used in the readout electronics.

As multiple TES are connected in parallel, the derivation of certain values are different compared to singular TES devices. For singular TES devices, one can read Callum's thesis, where that specific derivation is explained in greater detail [3]. To obtain the current going through the TES, we can use the following:

$$I_{TES} = V_{fb} \cdot F_{corr} \cdot gain \cdot \frac{1}{\sqrt{8}} \tag{1}$$

The last part comes from converting the I_{TES} value to its RMS equivalent. Plotting I_{TES} against V_{bias}, a slope R_{C_N} can be found. Combined with the slope of the superconducting region, R_{par}, the total voltage over the LC filter and the TES can be calculated:

$$V_{LC} = V_{bias} \cdot \frac{R_N R_{par}}{R_{C_N}} \tag{2}$$

As the total current over this part is equal to I_{TES}, the total resistance can be found with:

$$R_{LC} = \frac{V_{LC}}{I_{TES}} \tag{3}$$

Using equation 3, the TES resistance can be found. Together with equation 1, other important values can be calculated as follows:

$$R_{TES} = R_{LC} - R_{par} \tag{4}$$
$$V_{TES} = I_{TES} \cdot R_{TES} \tag{5}$$
$$P_{TES} = I_{TES} \cdot V_{TES} \tag{6}$$

The TES voltage is used for the characteristic IV curve, while the power provides information about the absorbed power via incident photons.

3.2 TES Behaviour

There are two main plots that provide important metrics about the TES and how its working. The first one is the Current - Voltage (IV) curve. Figure 3 shows such a plot, where two symmetric curves are visible divided by an almost vertical line. Single sided curves do not have this symmetry and hence need different ways to obtain certain values.

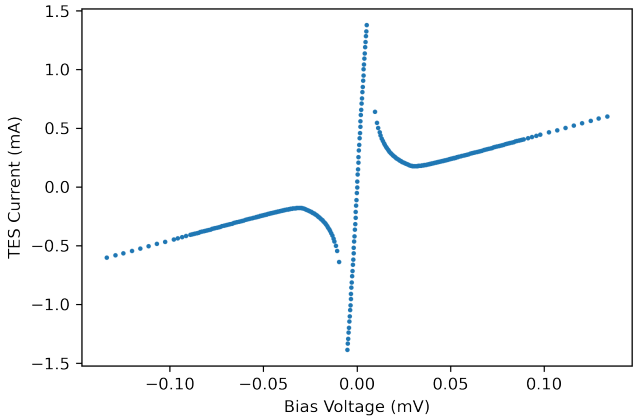

Figure 3: Plot of a double sided IV curve.

The central vertical line is the superconducting region, which is completely vertical when $R_{par} = 0$. Next is the transition region, which is the part where the curve is non-linear. The final section is the ohmic/normal region, which are the outer linear parts. Finding the normal resistance of the TES (R_N) is done by fitting a line through the ohmic region.

The second important plot is the Power - Resistance (PR) curve. Two straight regions are visible, called power plateau's.

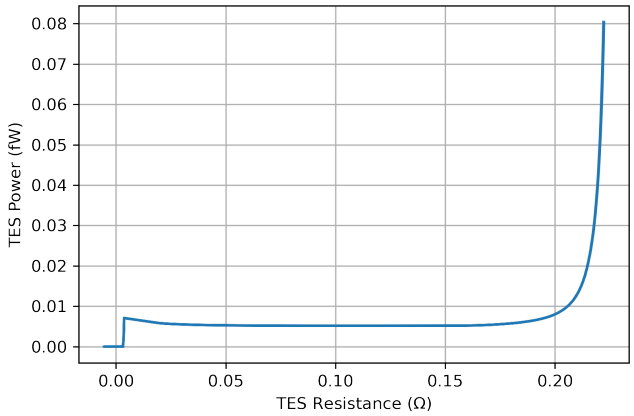

Figure 4: Plot of a Power - Resistance curve.

The vertical power plateau approaches the normal resistance R_N, and the horizontal one can be used as a value for the Joule power. The Joule power can also be definitions in other ways, like the power at the lowest point in the IV curve or the power at 80% of the normal resistance.

3.3 Existing Software

All work that will be done will be added to the already existing software created by Callum Blair. This software is already capable of reading the data files, creating plots and calculating values like the thermal conductance G and R_{TES} for a single TES detector. The software is written in python and it stores each data set in an `IV_curve` object. Multiple `IV_curve` objects can then be stored in a `IV_series` object, to easily access multiple data sets at once.

Work shall be done on extending the software to allow for single sided IV curves, which currently can not be analyzed properly. Some algorithms written by Callum require symmetry, which is obviously not present for single sided curves. Different algorithms will be required for finding the important parameters in these datasets.

Furthermore, the FDM datasets contain more information than the singular TES datasets, and hence the software will need additional functions and data reading methods to incorporate this information.

4 Results

4.1 Combining Previous Work

Callum and Arnold have made significant process on the work that needs to be done, however they produced two different pieces of software that did not work together. The first objective is to combine these two into a single one while sustaining the capability and flexibility of the individual software.

Arnold's work [10] consisted of 4 separate files, each of which performed a different function. These 4 functions were reading the data, creating training data, training a neural network and applying/testing the neural network. If data were to be analysed, all functions were dependent upon the output of their predecessor, therefore it made sense to combine them all into a single class.

The class is called `Classifier` and is implemented within the software Callum wrote. Data can now be analyzed by the `Classifier` class, where certain data sets are put into a separate directory. `IV_series` can then take that directory as its data input for further analysis. If no classification is necessary, then the software can be run as normal by not using the classifier and putting the directory straight into `IV_series`.

4.2 Fitting Single Sided Curves

After the `Classifier` class was implemented, it was possible to analyze the single sided IV curves. Single sided data sets were not available yet at the time of testing, therefore the double sided were transformed into single sided ones. Finding the edges of the superconducting regions was sufficient for this transformation, which where found by calculating a significant difference in gradient.

The benefit of using a part of the originally double sided curve is that they allow for easy comparison between the the accuracy of the old fitting method and tested ones, which are explained in the following sections.

4.2.1 Fitting Linear Function

The previous software version fits a single linear function through the first and last 10 points in the ohmic region of the double sided curves. To check if it would be beneficial to include more points, the amounts of points used for fitting the straight line were gradually increased. Simultaneously the residuals, defined as the differences in y-axis values between each point and the fitted line, were calculated to see if they started increasing.

Figure 5 shows such a plot for single sided IV curves. On the left side we can see an example of the amount of points taken to fit the straight line, in this case 30. Next to it is the distribution of the residuals.

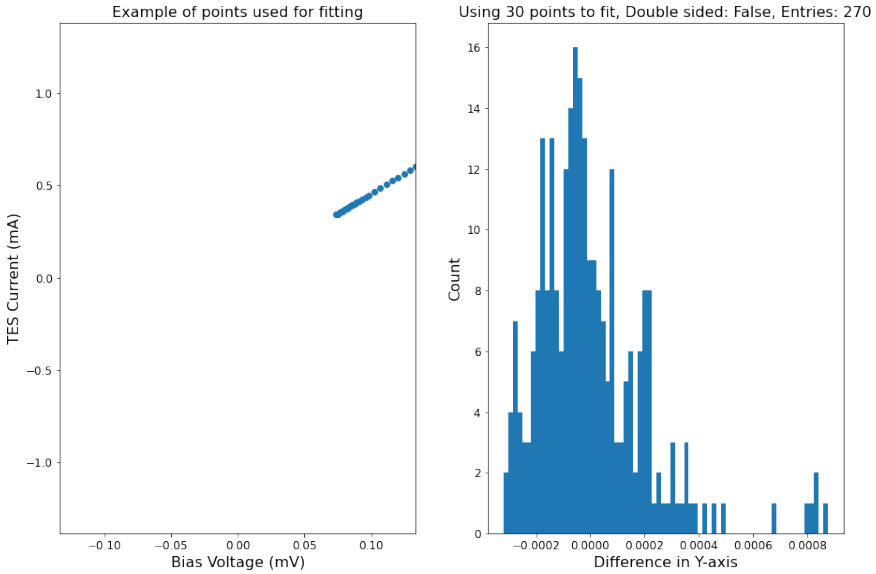

Figure 5: *(Left)* Example of points used for fitting. *(Right)* Y-axis difference between points and the fitted line.

Double sided fits were done by fitting one straight line through points of both sides of the curves, as was done in Callum's work. Figure 6 shows two peaks, neither of which is centered around zero.

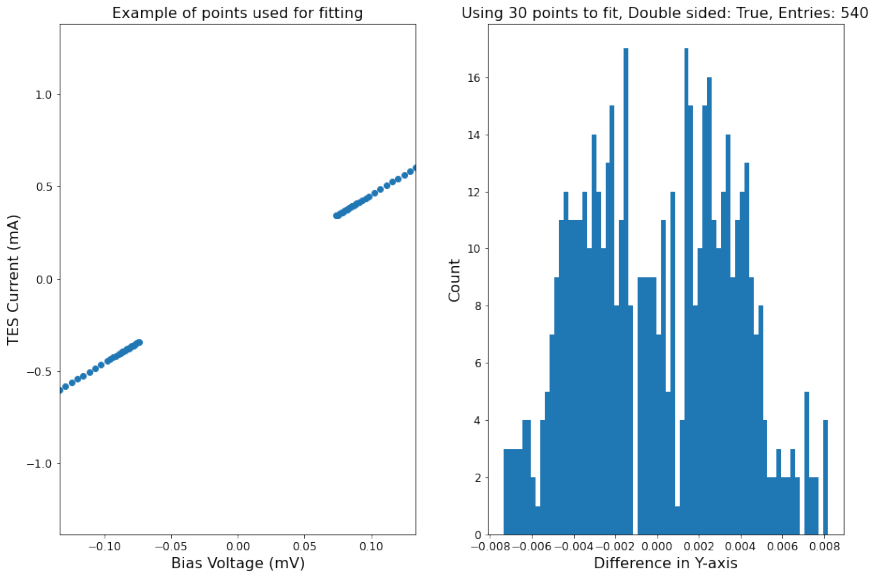

Figure 6: *(Left)* Example of points used for fitting. *(Right)* Y-axis difference between points and the fitted line.

One straight line misses both ohmic regions by a small margin, which is the center of the individual peaks. The IV curve is thus not fully symmetric and the curves should be fit separately for greater accuracy.

If a linear function would be a proper fit, the first distribution should represent a normal distribution. However, observing the picture reveals that the distribution is not

symmetric, as the distribution is right skewed. Either including 30 or more points is not suitable for fitting the function or a different function should be used. The second option is explored in section 4.2.2. Using 10 points, as was done by Callum, leads to less skewed results however using so few points makes the fitting procedure very sensitive to outliers.

4.2.2 Fitting Exponential Function

Linear fits showed distances that were skewed to one side of the line, resembling an exponential pattern. To prevent this, both single and double sided datasets were fitted to a model of the form:

$$f(x) = Ax + B + \frac{|x|}{x} C e^{-\frac{|x|}{x} D(x - x_0)} \tag{7}$$

These functions resemble both the ohmic and transition regions when using the right parameters. Also, if no exponential part would be present, C would just get set to zero and the function is linear again. Fitting equation 7 to the same single sided section as before, we obtain figure 7.

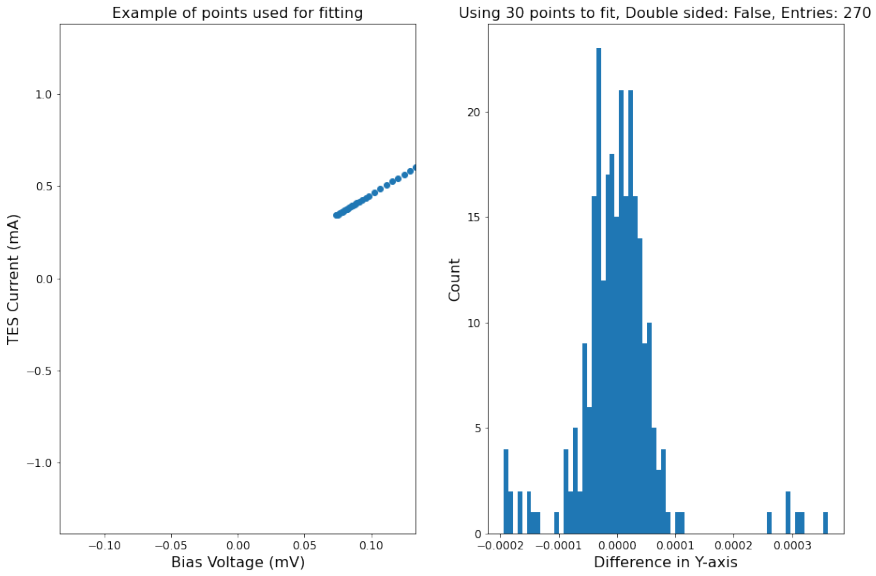

Figure 7: *(Left)* Example of points used for fitting. *(Right)* Y-axis difference between points and the fitted line.

Figure 7 shows a more symmetric distribution than the previous linear fits. The standard deviation is likely to be smaller, as a major part of the distribution lies within the range of [-0.0001, 0.0001] instead of [-0.00025, 0.0004].

Double sided fits were performed by fitting a single function on both sides and fitting two separate exponential functions on both sides. Figure 8 shows the result of one function being fitted to both sides using the same parameters. While one side is fitted properly, the other one is offset by some margin and hence requires a different set of parameters.

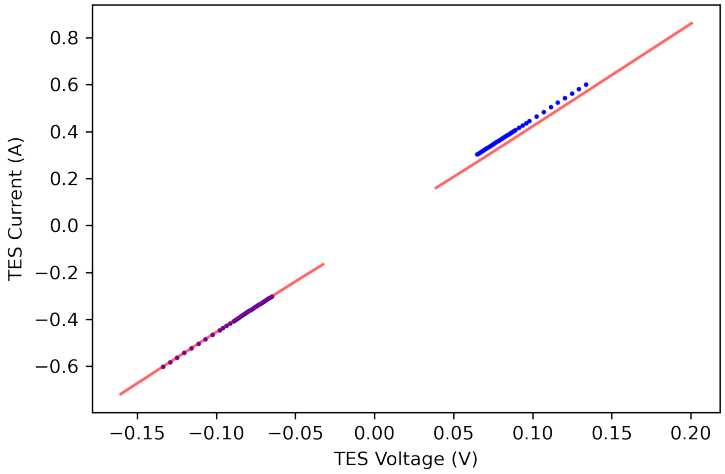

Figure 8: Example of how fitting function 7 to both sides.

Applying the exponential function to both sides separately leads to better results, due to asymmetries from the TES data. Finally, equation 7 was applied to both sides separately. These results are shown below.

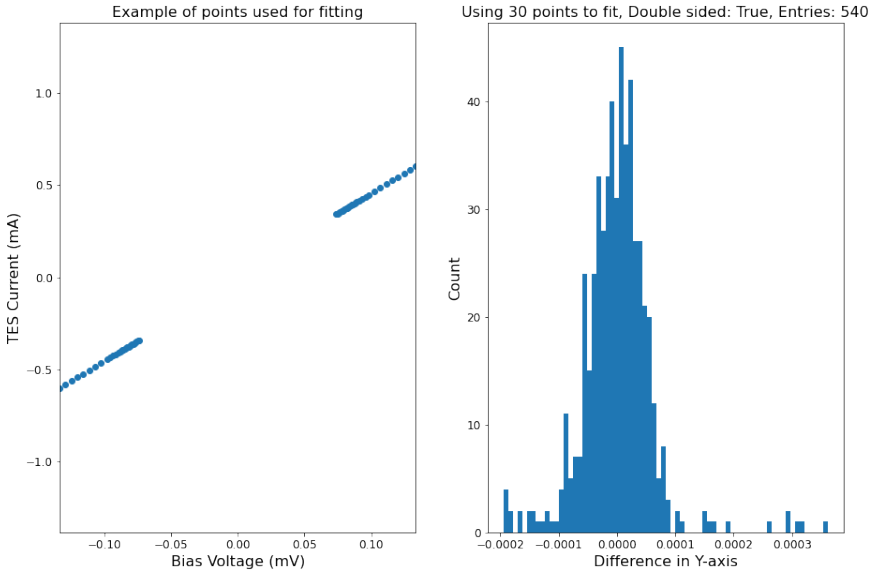

Figure 9: *(Left)* Example of points used for fitting. *(Right)* Y-axis difference between points and the fitted line. Separate exponential functions were fitted to each side.

A similar distribution to the one of figure 7 is visible, with a peak centered nicely around zero and the majority of points falling in between [-0.0001, 0.0001].

One source of error is that `scipy.optimize`, the fitting tool used, uses bounds for the parameters to obtain the right values. The bounds are necessary as increasing the total amount of parameter iterations (`maxfev`) did not always lead to a proper fit, even if set up to 10.000.000 or more iterations. If any new datasets include significantly dif-

ferent values, the bounds might be too narrow and the software might not be able to fit the function properly.

4.2.3 Fit Comparisons

Previous sections have shown that using an exponential function led to better accuracy of fitting the given data. However, only one sample size of 30 points was shown and comparing them is time consuming. To simplify these results, the standard deviation of the residual distributions were calculated. These standard deviations were plotted against the number of points used for fitting the curve, as shown in figure 10 below.

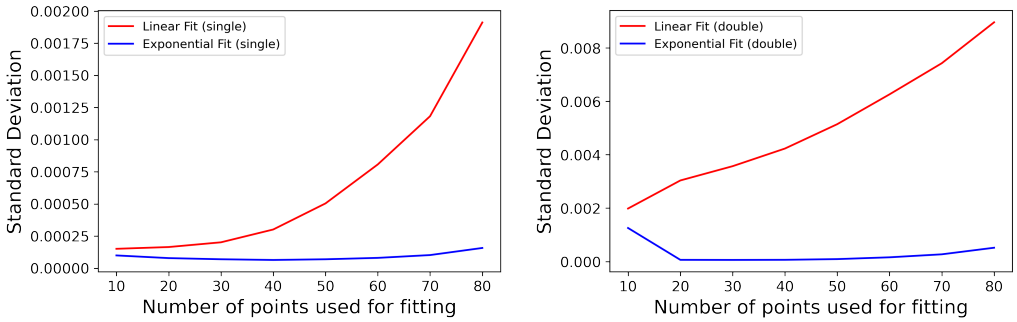

Figure 10: Plot of the standard deviation of the residual sample against the number of points used for fitting the single sided IV curve *(Left)* and the double sided IV curve *(Right)*.

Exponential fits are mostly unaffected by the amount of points taken during the fitting procedure, while the linear fits quickly grows to multiple times the initial standard deviation at 10 points.

Applying the exponential function allows the use of more points for fitting the curve, while not losing out on accuracy of the fit. This is important, as using more points leads to less error prone fits due to weird behaviour at the end of the IV curve. As the last part is far away from the thermal equilibrium of the system, it can be more sensitive which leads to errors. Furthermore, the exponential function is a better solution to fitting datasets containing no ohmic region, as the shape of Eq. 7 matches the start of the transition region well.

Other functions for fitting have not been tested, and might yield better results. The exponential fit works properly up to the point where the transition increases slightly, however including more points does not yield better fits. Some functions might fit properly to the whole curve, but further research or knowledge about the inherent physics of the system would be required.

4.2.4 Normal Resistance Shift

By implementing the exponential function to fit these curves, values like the calculated normal resistance R_N changed. The effects of this are shown in the image below.

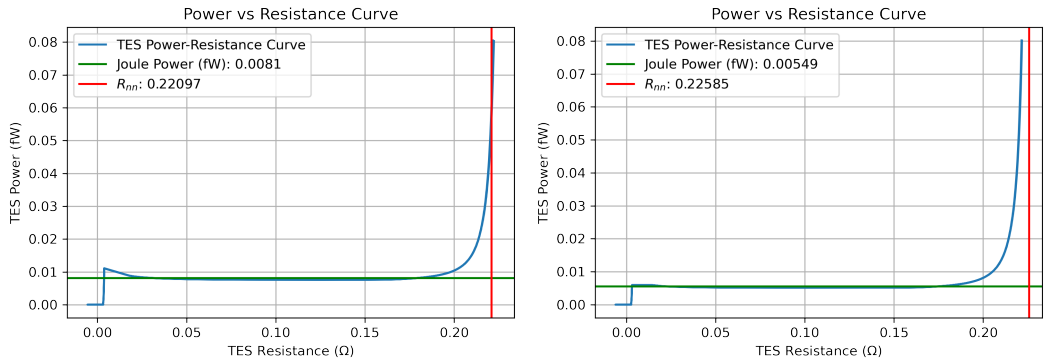

Figure 11: *(Left)* PR plot using the old fitting method. *(Right)* PR plot using the new fitting method. Both plots also show the calculated Joule power and normal resistance.

Applying the exponential fit leads to the normal resistance shifting to the right of the PR curve. This behaviour is observed for all datasets.

As the software will be used for calibration, and many properties are not known beforehand, comparing results based on numbers is difficult. However, looking at the produced graphs and output does provide useful information about the accuracy of the single sided analysis. For example, R_N shifting to the left of the PR curve makes sense, as the curve should approach the normal resistance but not exceed it. Only when running the experiment up to higher temperatures would you expect to exceed R_N, which is not the case for these measurements. Single sided PR curves show the same consistent behaviour.

4.3 Implementing Single Sided Analysis

Once the single sided IV curves became available, I started working on implementing these into the software. These single sided IV curves came from a FDM TES setup and hence they were structured differently than the singular TES data. The single sided curves were supplied as `.dat` files, and they contained a lot more parameters than the original double sided data.

To keep track of the differences between single sided and double sided curves, a separate class `IV_single` was created. The other class was renamed to `IV_double`, and each class has a separate data list in the `IV_series`. When supplying data to the software the user must enter whether the data is single sided or double sided, and `IV_series` automatically creates the appropriate data list, which can be looped over for access to individual datasets.

The `IV_single` class has mostly the same functionality as `IV_double`, except that some values are calculated differently. Furthermore, all parameters are stored inside a dictionary such that they can be stored and retrieved much simpler. Also, the Joule power is obtained by taking the power value at the lowest point in the IV curve instead of the value at the power plateau.

The `IV_series` class has obtained additional methods to calculate the absorbed power for each particular pixel and store these values in an array. These values can be plotted inside a grid, to show which pixel absorbed how much Joule power. Methods are now put under either double or single sided method, to clearly differentiate between the two.

4.3.1 Investigating Phase Data

FDM datasets also contain information about the current phase angle, read out by the SQUID. The generated alternating current is a sine wave. Figure 12 shows a slowly increasing phase angle. Two large jumps are present, which takes place in the final part of the superconducting region. No clear explanation is present for the occurrence of the first large gap, however it might be due to highly sensitive current in those temperature ranges. The second jump is a result from the system, as the phase gets reset to 180 degrees once it goes past -180 degrees.

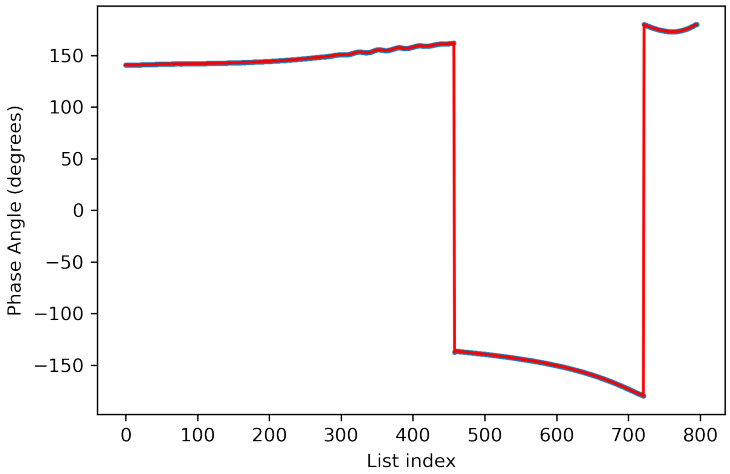

Figure 12: Plot showing the current phase angle in degrees, plotted in order from the first value to the last.

However, as this drop is present in the region where the superconducting region starts to bend and break linearity, it is not of great use. No information is gathered from that region so further inspection was not of great importance.

4.3.2 Important FDM Methods

The most important method of the new `IV_series` object is plotting the array of pixels combined with their measured absorbed Joule power with `plot_array`. Such an image contains the most important information when quickly analyzing the data from the whole system.

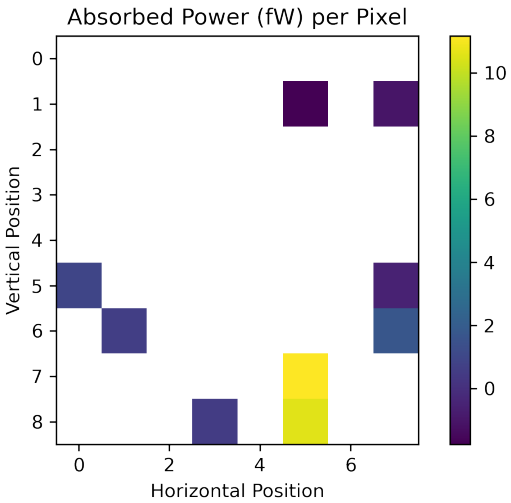

Figure 13: TES detectors displayed as pixels in the real order on the grid, displayed with the power difference between dark and optical mode.

Note that the data for each pixel was obtained separately from each other during measurements. The associated value with each pixel is the difference in Joule power between the dark and optical mode. For this measurement light reached the lower right corner, which is clearly visible from the image.

Additionally, for single pixel analysis in the FDM setup, the Joule power can be plotted for different black body temperatures. This can be done with the `plot_PT` method and a result is shown in the figure below:

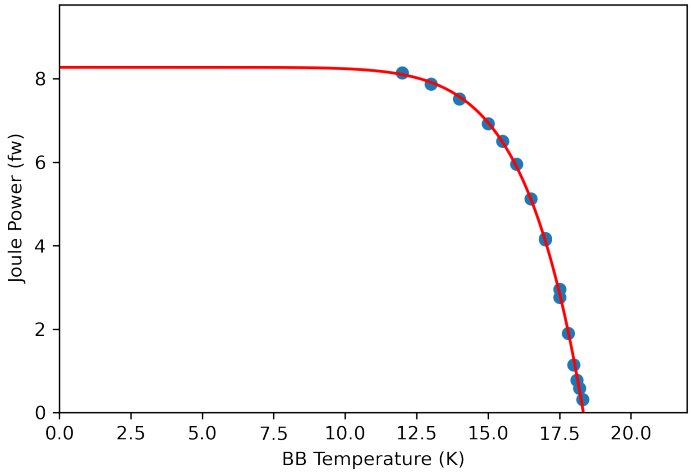

Figure 14: Calculated Joule power for different black body temperatures for a single pixel.

A power law is fitted to the data to check the expected behaviour of the data. Any outliers hint to incorrect data or unexpectedly behaving analysis and hence requiring further analysis.

Current datasets only use a few pixels during testing, but eventually all pixels on this grid will be active for measurements at the same time. Nearby pixels in the grid show similar absorbed power values. Pixels with no excitation show absorbed Joule powers around 0 fW as expected, however, some of these numbers are below zero. Deviations like these might be within error range, but error approximations are not present in the software and would be a great addition in future versions. Including error values would

require more information about the data and the order of magnitude of certain error sources.

The software behaves as expected, without inexplicable jumps between pixels. Figure 14 also shows that the software provides accurate analysis. Note that multiple datasets were present for the same low temperature, but they all differed in size and hence were neglected. Unfortunately not many datasets are currently present for analyzing the final grid output, complicating the accuracy checking of the software. From reading the 18 datasets, between sizes of 60 - 80 kB, to plotting the grid image takes roughly 10 seconds and thus is fast enough to process larger quantities of data sets. Most time is spent on the fitting procedure, as these FDM datasets contain more points in the ohmic region than the double sided ones. More efficient methods could be developed to fit Eq. 7 onto less points without losing out on accuracy, if total computing time becomes too long.

5 Software Limitations

The implementation and capabilities of Arnold's `Classifier` were difficult to test. Datasets used for testing the software are handpicked, as the whole FDM system is very sensitive, eliminating the use of any NN to separate datasets. Simple test were performed and successful, however its full use will need to be tested later on when more simultaneous test runs are done.

The software is also not tested on datasets where multiple pixels are tested simultaneously. Datasets used during testing read out a single pixel each time, as the cross talk between pixels significantly affects the data. Further research and testing will need to be done before multiple pixels will be read out at the same time with consistent results. This likely will require additional methods to deal with certain inconsistencies or additional parameters, as it was not possible to test the software on these kinds of datasets.

Lastly, the software is designed to read out data in a specific order. If the columns of the feedback and bias voltage were to change in some dataset, the software will remain analyzing as if that were not the case. More generalizable data reading methods would help the software, as the collected data changes from time to time. It also assumes the data to be in mV and any change in units goes unnoticed by the current methods used.

6 Conclusion

The requests for the software's functionality, as described in the introduction, are satisfied. The software is able to analyze single sided IV curves from the FDM setup with minimal user effort. All of this is done in a short time span, without the need of any advanced computational hardware. Double sided IV curves analysis has stayed the same, except for the implementation of an exponential function (Eq. 7) instead of the previous linear function.

The exponential fit proved to accurately approximate the R_N value of the TES in the FDM setup, as well as provide a more reasonable value in the double sided data. Considerably more data points can be used to smooth out outliers and are less error-prone. Investigation of the phase data led to no interesting information, and hence was not incorporated in the FDM analysis.

The software can be found on github:
`https://github.com/TomR21/TES-Analysis-Program`.
Additional documentation was added during development and the github link contains a walk through of the software to explain the basics usage and fundamentals.

Further research towards the physics of the TES sensor and how it behaves in the FDM system can benefit the software greatly, by providing better results comparisons and testing multiple active pixels simultaneously. Additionally, it could lead to better models for fitting the IV curves.

Lastly, any additional utilities for the different classes, like error estimation or utilizing noise spectra, are always welcome.

7 Acknowledgements

I am greatly thankful towards Damian Audley for his help on the subject and the questions that I had, along with Myroslav Kavatsyuk for all the insightful questions and feedback during this thesis. I also want to thank them both for their guidance through this project. Furthermore, I want to thank SRON for lending me the opportunity to be able to work on this exciting project.

References

[1] SRON. *Athena / X-IFU*. Accessed: 14-9-2021. URL: `https://www.sron.nl/missions-astrophysics/athena`.

[2] F. Pajot et al. "The Athena X-ray Integral Field Unit (X-IFU)". In: *Journal of Low Temperature Physics* 193.5 (2018), pp. 901–907.

[3] C. Blair. "Design of Software Routines for Automatic Calibration of Transition Edge Sensors". Bachelor Thesis. University of Groningen, 2019.

[4] B. Cabrera. "Introduction to TES Physics". In: *Journal of Low Temperature Physics* 151.1 (2008), pp. 82–93.

[5] P. Atkin, J. de Paula, and J. Keeler. "Atkins' Physical Chemistry". In: vol. 11. Oxford University Press, 2018. Chap. 15. ISBN: 978–0–19–108255–9.

[6] K. D. Irwin. "SQUIDs and Transition-Edge Sensors". In: *Journal of Superconductivity and Novel Magnetism* 34.6 (2021), pp. 1601–1606.

[7] J. N. Ullom and D. A. Bennett. "Review of superconducting transition-edge sensors for x-ray and gamma-ray spectroscopy". In: *Superconductor Science and Technology* 28.8 (2015), p. 084003.

[8] R. A. Hijmering et al. *Readout of a 176 pixel FDM system for SAFARI TES arrays*. 2016.

[9] M. D. Audley et al. "Performance of a Low-Noise Test Facility for the SAFARI TES Bolometer Arrays". In: *Journal of Low Temperature Physics* 167 (2012), pp. 208–213.

[10] A. Dongelmans. "Testing the X-IFU Focal Plane Assembly: PID Temperature Control & Applying Machine Learning to Detector Classification". Internship Report. SRON, 2020.